ACCOUNTS
of chemical research

Fresh Look at Electron-Transfer Mechanisms via the Donor/Acceptor Bindings in the Critical Encounter Complex

SERGIY V. ROSOKHA AND JAY K. KOCHI*

Department of Chemistry, University of Houston, Houston, Texas 77204

RECEIVED ON NOVEMBER 26, 2007

CONSPECTUS

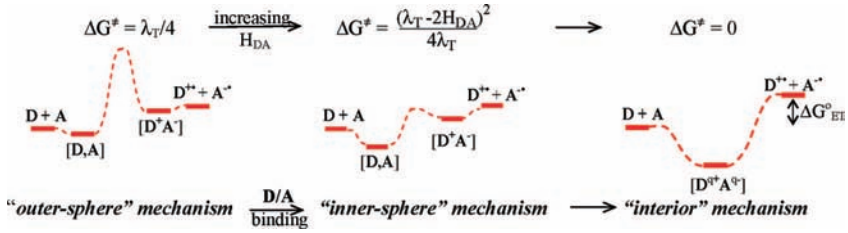

Seminal insights provided by the iconic R. S. Mulliken and his "charge-transfer" theory, H. Taube and his "outer/inner-sphere" mechanisms, R. A. Marcus and his "two-state non-adiabatic" theory, and N. S. Hush and his "intervalence" theory are each separately woven into the rich panoramic tapestry constituting *chemical research into electron-transfer dynamics*, and its mechanistic dominance for the past half century and more. In this Account, we illustrate how the simultaneous melding of all four key concepts allows sharp focus on the charge-transfer character of the critical encounter complex to evoke the latent facet of traditional electron-transfer mechanisms. To this end, we exploit the intervalence (electronic) transition that invariably accompanies the diffusive encounter of electron-rich organic donors (D) with electron-poor acceptors (A) as the experimental harbinger of the collision complex, which is then actually isolated and X-ray crystallographically established as loosely bound π-stacked pairs of various aromatic and olefinic donor/acceptor dyads with uniform interplanar separations of $r_{DA} = 3.1 \pm 0.2$ Å. These X-ray structures, together with the spectral measurements of their intervalence transitions, lead to the pair of important electron-transfer parameters, H_{DA} (electronic coupling element) versus λ_T (reorganization energy), the ratio of which generally defines the odd-electron mobility within such an encounter complex in terms of the resonance stabilization of the donor/acceptor assembly [D, A] as opposed to the reorganization-energy penalty required for its interconversion to the electron-transfer state [$D^{+\bullet}$, $A^{-\bullet}$]. We recognize the resonance-stabilization energy relative to the intrinsic activation barrier as the mechanistic binding factor, $Q = 2H_{DA}/\lambda_T$, to represent the quantitative measure of the highly variable continuum of inner-sphere/outer-sphere interactions that are possible within various types of precursor complexes. First, $Q \ll 1$ identifies one extreme mechanism owing to slow electron-transfer rates that result from the dominance of the intrinsic activation barrier (λ_T) between the encounter and successor complexes. At the other extreme of $Q \geq 1$, the overwhelming dominance of the resonance stabilization (H_{DA}) predicts the odd-electron mobility between the donor and acceptor to occur without an activation barrier such that bimolecular electron transfer is coincident with their diffusional encounter. In between lies a potentially infinite set of states, $0 < Q < 1$ with opposing attractive and destabilizing forces that determine the location of the bound transition states along the reaction coordinate. Three prototypical potential-energy surfaces evolve as a result of progressively increasing the donor/acceptor bindings (H_{DA}) extant in the precursor complex (at constant λ_T). In these cases, the "outer-sphere" mechanism is limited by the weak donor/acceptor coupling that characterizes the now classical Marcus outer-sphere mechanism. Next, the "inner-sphere" mechanism derives from moderate (localized) donor/acceptor bindings and includes the mechanistic concept of the bridged-activated complex introduced by Taube for a wide variety of ligand-based redox dyads. Finally, the "interior" mechanism is also another subclass of the Taube (inner-sphere) classification, and it lies at the other extreme of very fast electron-transfer rate processes (heretofore unrecognized), arising from the spontaneous annihilation of the donor/acceptor dyad to the delocalized (electron-transfer) complex as it descends barrierlessly into the chemical "black hole" that is rate-limited solely by diffusion.

Published on the Web 04/02/2008 www.pubs.acs.org/acr
10.1021/ar700256a CCC: $40.75

1. Historical Perspective

Electron-transfer concepts that originate from the confluence of four major insights commencing 50 or so years ago pervade the modern development of fast chemical dynamics. Initially, Mulliken[1] conceived the diffusional interaction of an electron-rich donor (D) with a relatively electron-poor acceptor (A) to form reversibly the encounter complex [D,A] that is spontaneously observed as vivid colors related to the optical (charge-transfer) transition identified in eq 1.

$$D + A \overset{\text{diffuse}}{\rightleftharpoons} [D, A] \overset{h\nu_{CT}}{\rightleftharpoons} [D^{+\bullet}, A^{-\bullet}] \qquad (1)$$

Almost simultaneously, the mechanistic classification of inorganic electron transfers of mostly octahedral (coordination) complexes was formulated by Taube[2] based on a pair of distinct and separate pathways involving outer-sphere (OS) and inner-sphere (IS) processes in which the critical encounter complexes can be qualitatively differentiated as depicted in eq 2.

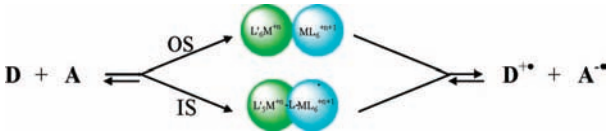

(2)

The theoretical development of intermolecular electron transfer followed a few years later as a result of Marcus' formulation[3] that was inspired by Taube's depiction of outer-sphere electron transfer in which the activation barrier was identified with the non-adiabatic or weakly adiabatic interconversion between the encounter (or precursor) complex and the successor complex, that is,

$$D + A \overset{\text{diffuse}}{\rightleftharpoons} [D, A] \overset{\text{ET}}{\rightleftharpoons} [D^{+\bullet}, A^{-\bullet}] \overset{\text{diffuse}}{\rightleftharpoons} D^{+\bullet} + A^{-\bullet} \qquad (3)$$

Most interestingly, the Marcus formulation of bimolecular electron transfer according to eq 3 shares a common path with Mulliken's concept of non-adiabatic electron transfer via the diffusion-controlled donor/acceptor preequilibrium step in eq 1. Indeed, Hush[4] simultaneously recognized the charge-transfer transition in eq 1 as the signal earmark of the important donor/acceptor electronic coupling (H_{DA}) that characterizes the [D, A] associate, and his independent development of intervalence electron-transfer theory otherwise (more or less) paralleled Marcus theory.

The intense and successful experimental validations of Marcus theory over the ensuing 40 or more years have largely focused on the electron-transfer behavior of weakly coupled (octahedral) redox dyads with $H_{DA} < 200$ cm^{-1}, so that the computational task is considerably facilitated to approximate the non-adiabatic or weakly adiabatic limitations of the outer-sphere electron-transfer mechanism.[3,5] By contrast, studies of adiabatic electron-transfer processes that characterize the inner-sphere mechanism[2] are singularly bereft of quantitative (theoretical) insights. The latter is somewhat understandable when one considers the experimental difficulty of rigorously identifying the structural parameters required by the actual isolation of the heretofore putative (intimately bound) inner-sphere encounter complex, especially in fast bimolecular electron transfers. [Note that such a limitation is not imposed on outer-sphere electron transfer because the requisite structural parameters of the loosely bound precursor complex (such as they are) are obtained from the readily accessible and intact reactants and products.]

Our interest in electron-transfer concepts derives from a different perspective, the focus being centered on the bimolecular interaction of organic electron donors (as nucleophiles) and electron acceptors (as electrophiles).[6] Especially important is the widely applied Mulliken theory that provides three important experimental probes that can be invoked in the diffusion-controlled formation of the "collision" or encounter complex, hereinafter referred to generically as the *charge-transfer complex* in eq 1, namely, (1) the instantaneous spectroscopic identification and characterization of [D, A],[1,7a,b] (2) their isolation and X-ray structures,[7c] and (3) the laser-induced optical (non-adiabatic) excitation of the HOMO–LUMO transition by time-resolved spectroscopy.[8]

Although the conceptual relationship between the Mulliken (charge-transfer) formulation in eq 1 and Marcus electron-transfer theory in eq 3 may seem to be obvious, for some unknown reason their *direct* (experimental) interrelationship has never been rigorously established. Accordingly, we begin this Account with the experimental demonstration of how the charge-transfer complex unambiguously relates to the adiabatic electron-transfer process. For our studies, Table 1 contains some prototypical electron donors (D) and electron acceptors (A) that are comprised of aromatic or olefinic redox centers with one or more unsaturated C–C bonds, together with their acronyms to facilitate their ready identification. In every case, the associated one-electron oxidation products ($D^{+\bullet}$) or reduction products ($A^{-\bullet}$) are all persistent cation or anion radicals and structurally characterized (X-ray) so that the free-energy changes for electron transfer are readily obtained from the relevant oxidation (E^0_{ox}) or reduction (E^0_{red}) potentials in Table 1.[9]

TABLE 1. Some Prototypical Electron Donors and Electron Acceptors

Donor		E^{o}_{ox} [a]	Acceptor		E^{o}_{red}
	**TMPD**	0.12		**DDQ**	0.52
	**TTF**	0.37		**DBQ**	0.50
	**PTZ**	0.59		**TCNE**	0.17
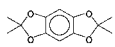	**TMDO**	0.74		***o*-CA**	0.15
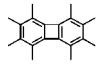	**OMB**	0.82	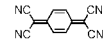	**TCNQ**	0.10
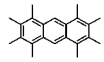	**OMA**	0.88		***p*-CA**	-0.02
	**DMB**	1.17	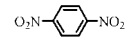	**DNB**	-0.64[b]

[a] Given in V vs SCE in dichloromethane at 22 °C. [b] In tetrahydrofuran.

2. Spectral Detection and X-ray Structures of "Collision" Charge-Transfer Complexes

Instantaneous coloration observed during the very fast (diffusive) encounter of an electron donor (D) with an electron acceptor (A) in solution,[7a] as well as in the gas phase,[7b] augurs the formation of the "collision" complex [D, A]. The first report of such a transient 1:1 complex is that between the benzene donor and the dibromine acceptor,[10] which constitutes the experimental basis for the Mulliken's development of charge-transfer theory,[1] the ground- and excited-state wave functions being formulated as

$$\Psi_{GS} = a\Psi_{D,A} + b\Psi_{D^+\cdot A^-\cdot} \quad \text{and} \quad \Psi_{ES} = b\Psi_{D,A} - a\Psi_{D^+\cdot A^-\cdot} \tag{4}$$

so that the optical color derives from the nonadiabatic $\Psi_{GS} \rightarrow \Psi_{ES}$ transition. Most noteworthy is the subsequent isolation and X-ray structure in Chart 1 of this and some related charge-transfer complexes in which the degree of charge transfer q (roughly corresponding to the normalization ratio b/a from eq 4) increases with donor and acceptor strength and can even approach unity (100%).[11]

3. Reversible Interchange of Charge-Transfer versus Electron-Transfer States

Of the various donor/acceptor combinations available from Table 1, we focus on those D/A dyads in which the electron-transfer driving force is close to isergonic, that is, $-\Delta G_{ET} = F(E^0_{red} - E^0_{ox}) \approx 0$, to represent the optimum combination for the equitable balance between charge-transfer and electron-transfer observations.[12]

A. Charge-Transfer State. Immediately upon mixing the colorless solution of the 2,2,6,6-tetramethylbenzo[1,2-*d*:4,5-*d'*]bis[1,3]dioxole (TMDO) donor with that of the 2,3-dichloro-5,6-dicyano-*p*-benzoquinone (DDQ) acceptor in dichloromethane, the mixture turns bright green, and the new characteristically broad near-IR band appears, the absorption change with concentration and temperature (Figure 1A,B) of which coincides with the reversible equilibrium in eq 5.[12]

$$\text{TMDO} + \text{DDQ} \overset{K_{CT}}{\rightleftharpoons} [\text{TMDO, DDQ}] \tag{5}$$

The experimental formation constant of the charge-transfer complex is established as $K_{CT} = 5.0$ at 15 °C with the typical thermodynamic parameters: $\Delta H_{CT} = -8$ kcal M^{-1}, and

CHART 1

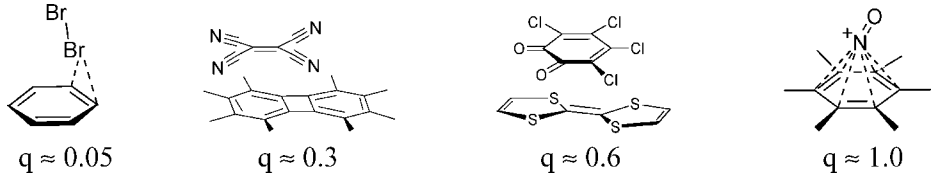

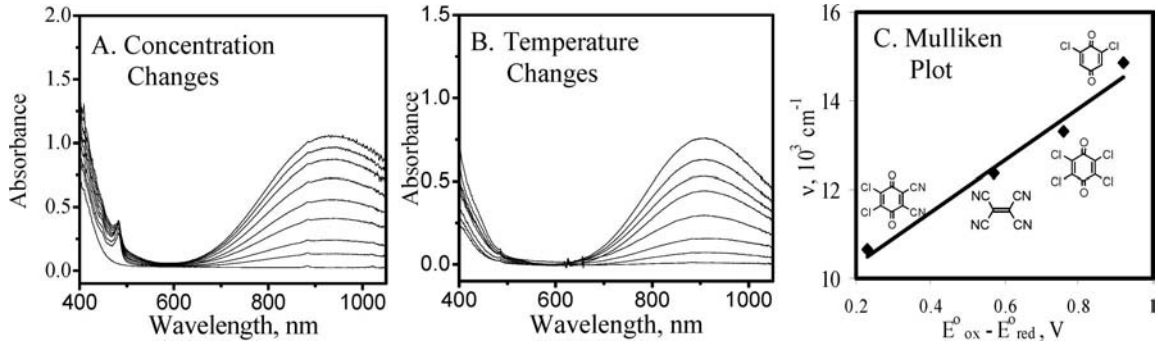

FIGURE 1. Concentration (A) and temperature (B) dependence of the intervalence absorption of [TMDO, DDQ] in dichloromethane and (C) Mulliken plot for TMDO complexes with various acceptors, as indicated.[12]

$\Delta S_{CT} = -25$ eu. The Mulliken correlation of the HOMO–LUMO gap, measured as $E^0_{ox} - E^0_{red}$ for TMDO in combination with various acceptors as indicated in Figure 1C, confirms the charge-transfer character of the new NIR absorption band.[12]

B. Solvent Dependence of the Electron-Transfer States. The use of more polar solvents such as acetonitrile or propylene carbonate (PC) in the bimolecular interaction of TMDO and DDQ at the same concentrations and temperature leads to the composite red spectrum in Figure 2 (left) principally consisting of the superposition of $D^{+\bullet}$ and $A^{-\bullet}$ (insets) diagnostic of the electron-transfer state, that is

$$\text{TMDO} + \text{DDQ} \overset{K_{ET}}{\rightleftharpoons} [\text{TMDO}^{+\bullet}, \text{DDQ}^{-\bullet}] \overset{\text{diffuse}}{\rightleftharpoons} \text{TMDO}^{+\bullet} + \text{DDQ}^{-\bullet} \quad (6)$$

following which the subsequent diffusive separation of the ion pair is rapid in these polar solvents.

C. Interchange of Electron-Transfer and Charge-Transfer States. Progressively lowering the temperature of the TMDO/DDQ solutions results in the gradual emergence of the characteristically broad charge-transfer spectrum in Figure 2 (right) at the expense of the electron-transfer spectrum. This, together with the clear isosbestic point at $\lambda_{iso} =$ 640 nm establishes the direct conversion of the electron-transfer state to the charge-transfer state. Thus these temperature modulations of the electron-transfer state, together with the preequilibrium in eq 6, provide unambiguous evidence for the facile and direct interchange with the charge-transfer state, that is,

$$[\text{TMDO}, \text{DDQ}] \overset{K_{CT/ET}}{\rightleftharpoons} \{\text{TMDO}^{+\bullet}, \text{DDQ}^{-\bullet}\} \quad (7)$$

Such a reversible interchange between the charge-transfer and electron-transfer states typically occurs with $K_{CT/ET} = 5.6 \times 10^4$ M^{-1} and the thermodynamic constants $\Delta H_{CT/ET} = 6$ kcal M^{-1} and $\Delta S_{CT/ET} = 5$ eu at 23 °C. [Note that our spectral studies do not distinguish among free ions, ion pairs, etc.]

4. Spectral Elucidation and X-ray Structures of the Critical Encounter Complex

The electron-transfer cross-exchange reactions between electron donors and acceptors (as in eq 6) with near isergonic driving forces thus provide the optimum opportunity to demonstrate the critical role of the charge-transfer complex to

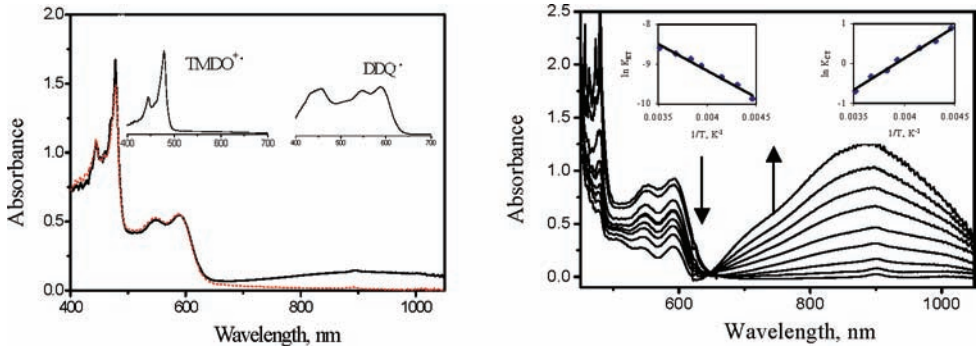

FIGURE 2. Electronic (UV-NIR) spectrum (left) of the electron-transfer state (black) as the spectral superposition (red) of $TMDO^{+\bullet}$ and $DDQ^{-\bullet}$ (insets) and temperature-dependent spectra (right) showing the simultaneous decrease of the electron-transfer state and increase of the charge-transfer state.[12]

represent the encounter complex in bimolecular electron transfers, that is,

$$D + A \rightleftarrows [D, A] \rightleftarrows D^{+\bullet} + A^{-\bullet} \quad (8)$$

A. Chemical Kinetics. The chemical kinetics of such a dynamic system, however, are experimentally difficult to evaluate quantitatively. Accordingly, we turn to the equivalent half-reactions in the form of the simplest electron-transfer counterparts, that is,

$$D + D^{+\bullet} \rightleftarrows D^{+\bullet} + D \quad \text{and} \quad A^{-\bullet} + A \rightleftarrows A + A^{-\bullet} \quad (9)$$

in order to study the corresponding self-exchange mechanism since they are both constrained to $-\Delta G_{ET} = 0$. Most importantly, Weissman and co-workers[13] earlier showed how the kinetics of such fast self-exchanges can be accurately monitored by magnetic resonance measurements involving EPR line-broadening. Figure 3 typically illustrates the progressive

FIGURE 3. Progressive line-broadening of the EPR spectra of $DDQ^{-\bullet}$ accompanying incremental addition of DDQ.

line-broadening of the EPR spectrum of $DDQ^{-\bullet}$ attendant upon the successive addition of DDQ in the slow-exchange limit leading to the collapse into one line, which is then narrowed in the fast-exchange limit to provide the unambiguous second-order rate constant of $k_{SE} = 2.5 \times 10^9\ M^{-1}\ s^{-1}$ at 23 °C in eq 10,[9] and the temperature dependence of k_{SE} yields the

$$DDQ^{-\bullet} + DDQ \rightleftarrows DDQ + DDQ^{-\bullet} \quad (10)$$

experimental activation energy for electron transfer as E_a = 1.6 kcal mol^{-1}.

B. Spectral Identification of the Transient Encounter Complex. The simultaneous monitoring of the EPR changes in Figure 3 by the independent examination of the electronic spectra in Figure 4 reveals the appearance of a new absorption band in the near-IR region with its maximum at λ_{CT} = 1406 nm ($\epsilon_{CT} = 3 \times 10^3\ M^{-1}\ cm^{-1}$). The absorbance increase with successive additions of DDQ confirms the reversible formation of the charge-transfer complex with K_{CT} = 11 M^{-1}, the temperature dependence of which affords $\Delta H_{CT} = -3.2$ kcal mol^{-1} and $\Delta S_{CT} = -6$ eu. It is important to note that the spectral characteristics of the new (red-shifted) NIR absorption band shown in Figure 4 (left) mirror those of the broad charge-transfer absorption in Figure 1, and thus it is likewise assigned to the intermolecular electronic transition in the charge-transfer complex,[9,14] that is,

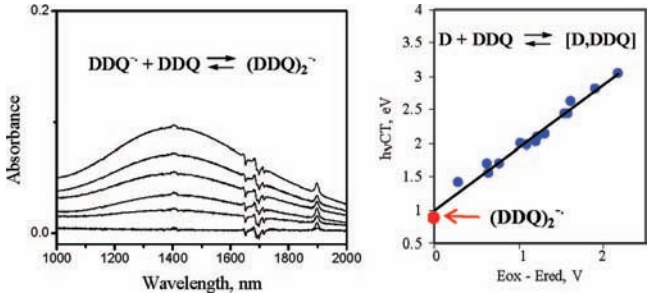

FIGURE 4. Increase of the NIR spectrum (left) of $(DDQ)_2^{-\bullet}$ accompanying the addition of DDQ to $DDQ^{-\bullet}$ and Correlation (right) of the $(DDQ)_2^{-\bullet}$ intervalence band (red arrow) vs Mulliken plot of other DDQ charge-transfer complexes with various donors (D, in blue), from ref 14.

$$DDQ^{-\bullet} + DDQ \overset{K_{CT}}{\rightleftharpoons} [DDQ^{-\bullet}, DDQ] \xrightarrow{h\nu_{IV}} [DDQ, DDQ^{-\bullet}] \quad (11)$$

and the new NIR absorption will be hereinafter referred to as the *intervalence* transition.

C. X-ray Structure of the Encounter Complex. When the equimolar solution containing $DDQ^{-\bullet}$ and DDQ in dichloromethane is cooled to −65 °C and carefully overlaid with hexane, it deposits dark brown crystals of the 1:1 precursor complex, the X-ray crystallographic analysis of which indicates the singly (negative) charged dimeric unit of a pair of cofacial DDQ moieties lying atop of each other (but slightly slipped) at the interplanar separation of r_{DA} = 2.95 Å, as shown in Figure 5. The C−C bond length analysis of the DDQ

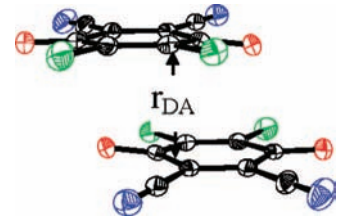

FIGURE 5. ORTEP diagram of the cofacially stacked $(DDQ)_2^{-\bullet}$ with interplanar separation of r_{DA} = 2.95 Å.

moieties in the dimeric anion relative to those extant in separate $DDQ^{-\bullet}$ and DDQ units indicates that the unpaired electron is distributed more or less equally between each half. Indeed, the cofacially stacked dimeric units characterize the structure of all precursor complexes isolated heretofore (Table 2).[15] Most importantly, the interplanar separation in every case lies within a rather narrow range of $r_{DA} = 3.1 \pm 0.3$ Å, which is significantly larger than any covalent-bonding distances but approximately 0.3 Å closer than the sum of their van der Waals separation, independent of whether the 1:1 precursor complex bears a single negative charge from an

TABLE 2. X-ray Structures of Ion-Radical and Charge-Transfer Complexes[15]

Dyads	Structure	r_{DA}, Å	Dyads	Structure	r_{DA}, Å
$(DBQ)_2^{-\bullet}$	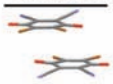	3.03	$(OMB)_2^{+\bullet}$		3.40
$(DDQ)_2^{-\bullet}$	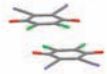	2.95	$(OMA)_2^{+\bullet}$		3.37
$(TCNE)_2^{2-}$		2.88	$(TTF)_2^{2+}$		3.40
$(TCNQ)_2^{-\bullet}$	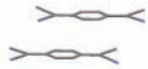	3.17	$(NAP)_2^{+\bullet}$		3.17
[DDQ,TMDO]	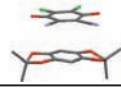	2.95	[*o*CA,TTF]	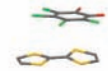	3.25

anionic donor (i.e., $A^{-\bullet}$ and A) or a single positive charge from a cationic acceptor (i.e., $D^{+\bullet}$ and D) as in eq 9. It is also important to note that Table 2 includes the X-ray structures of the charge-transfer complex of the TMDO/DDQ dyad that is involved in the electron-transfer cross reaction described in eqs 5 and 6. Striking are the strong similarities of the cofacial structures, with essentially the same r_{DA} values among all precursor complexes, irrespective of whether they are involved in the electron-transfer cross reaction (eq 8) or in the constituent self-exchange processes (eq 9).

5. Electronic Structures of the Encounter Complex

The diagnostic intervalence transition, together with the X-ray structure, provides the key to unraveling the electronic structure of the precursor complex. According to Mulliken,[1] the $\pi-\pi$ stacking of monomeric donor/acceptor units in the precursor complex (Figure 5) favors the electronic coupling of their frontier orbitals, which in the case of neutral [D, A] is the HOMO/LUMO, with the cationic $D_2^{+\bullet}$ is the HOMO/SOMO, and in the case of anionic $A_2^{-\bullet}$ is the SOMO/LUMO, as graphically illustrated in Chart 2, where the arrows represent the energy gaps of the bonding/antibonding orbitals.

CHART 2

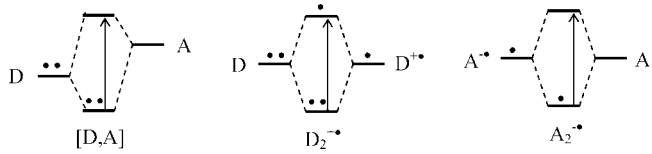

The electron-transfer barriers in such precursor complexes according to the two-state Marcus/Hush theory[1,2,5] derive from two opposing parameters: (a) the reorganization energy (or intrinsic barrier), λ_T, and (b) the electronic coupling element (or resonance stabilization), $2H_{DA}$. As a result, two (extreme) types of precursor complexes are to be expected, those in which $\lambda_T/H_{DA} > 2$ and those in which $\lambda_T/H_{DA} < 2$, and these belong to class II and class III, respectively, according to the classical Robin–Day classification of mixed-valence complexes.[16] It follows that the potential-energy surface for self-exchange in class II systems consists of a pair of isergonic ground states whereas only a single broad ground state pertains to class III systems, as graphically depicted in Chart 3.

CHART 3

In class II self-exchanges, the electronic coupling element can be obtained from the intervalence transition via the Hush relationship:[4]

$$H_{DA} = 0.0206(\nu_{IV}\Delta\nu_{1/2}\epsilon_{IV})^{1/2}/r_{\pi} \qquad (12)$$

where $\Delta\nu_{1/2}$ is a full width at half-maximum (cm^{-1}) of the NIR absorption band, ϵ_{IV} is its extincttion coefficient (M^{-1} cm^{-1}), and r_{DA} is the separation (Å) between the donor/acceptor centers. Likewise, the reorganization energy is equated to the intervalence transition: $\lambda_T = \nu_{IV}$.[5] Of the various $D/D^{+\bullet}$ and $A^{-\bullet}/A$ dyads we have examined, the analysis of intervalence transitions indicate that $\lambda_T = 7000$ and 5000 cm^{-1} for the $TCNE^{-\bullet}$/TCNE and $TTF/TTF^{+\bullet}$ dyads (TCNE = tetracyanoethylene and TTF = tetrathiafulvalene), respectively, and for the same pairs, $H_{DA} = 1100$ and 1600 cm^{-1}, so that electron transfer within these localized precursor complexes must occur

TABLE 3. Comparison of the Theoretical and Spectral Evaluations of the Coupling Elements[15]

$D_2^{+\bullet}$ or $A_2^{-\bullet}$	ν_{IV}, 10^3 cm^{-1}	R-D class	H_{DA}(spectral),[b] 10^3 cm^{-1}	H_{DA}(theor),[c] 10^3 cm^{-1}
$(OMB)_2^{+\bullet}$	5.5	III	2.8	2.3
$(OMA)_2^{+\bullet}$	4.1	III	2.0	1.5
$(TTF)_2^{+\bullet}$	~5.3[a]	II	(1.6)	3.6
$(NAP)_2^{+\bullet}$	9.5	III	4.8	4.6
$(TCNE)_2^{-\bullet}$	~7.0[a]	II	(1.1)	4.2
$(DDQ)_2^{-\bullet}$	~7.5[a]	II [III][d]	3.7 (1.8)	3.4
$(DBQ)_2^{-\bullet}$	~7.1[a]	II [III][d]	3.5 (1.8)	2.9
$(TCNQ)_2^{-\bullet}$	4.5	II [III][d]	2.3 (1.4)	1.9

[a] Solvent dependent. [b] As $H_{DA} = \nu_{IV}/2$ or via eq 12, in parenthesis. [c] B3LYP/6-311G*. [d] Brackets reflect our uncertainty in the assignment to either class II or III.

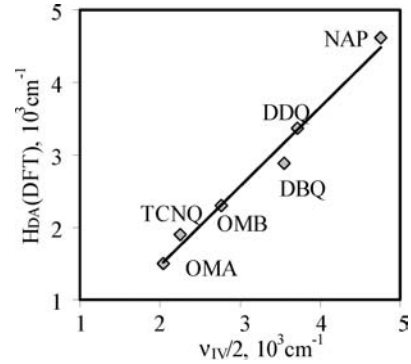

FIGURE 6. Concordance of the theoretically calculated (DFT) H_{DA} versus the experimental H_{DA} evaluated from the NIR absorption bands.[15]

reversibly by the odd-electron hopping between the two equivalent energy minima illustrated in Chart 3 (left).

According to the two-state Mulliken–Hush formulation, the intervalence transition provides direct insight into the fully delocalized electronic structure illustrated in Chart 3 (right) of the class III precursor complex for self-exchange, that is, $\nu_{IV} = 2H_{DA}$.[17] The values of H_{DA} are listed in Table 3, together with those evaluated for the corresponding class II complexes (vide supra).

Let us now establish how theoretical insight will validate the electron-transfer parameters that are experimentally measured from the intervalence spectral data.

6. Theoretical Computation/Validation of the Electron-Transfer Parameters for Robin–Day Class II and III Encounter Complexes

A. Computation of H_{DA}. The theoretical treatment of the electronic coupling elements for the precursor complexes is based on the energy splitting according to Mulliken of the symmetric and antisymmetric orbital combinations in Chart 2[18] at the *ab initio* Hartree–Fock level with the 6-311G* basis set and by DFT calculations (B3LYP). The computations of the orbital energies are taken from the orthogonal (X-ray) coordinates and one-half of the difference of the highest symmetric and antisymmetric occupied orbitals, and these correspond to the values of H_{DA} for $D_2^{+\bullet}$ (Table 3). The same is applied to the lowest symmetric and antisymmetric virtual orbitals as employed in the computations of H_{DA} for $A_2^{-\bullet}$. The concordance of the calculated values of H_{DA} with the corresponding experimental (intervalence) values based on $H_{DA} = \nu_{IV}/2$ is illustrated in Figure 6 for a series of Robin–Day class III precursor complexes; and this provides the unmistakable validation of the two-state Mulliken–Hush theory to correctly predict the electronic structures of the intermolecular encounter complex, especially for the strongly bound class III systems. For the more weakly coupled class II analogues, the agreement is less precise largely owing to the ambiguities as to the applicability of the separation parameter r_{DA} determined from the solid-state data. For such, the discrepancy is attributed to the less-constrained librational movements between monomeric moieties that are possible for these unusually long-bonded precursor complexes in solution.[19]

B. Computations of λ_T. According to Marcus,[3] the intrinsic barrier, λ_T, for intermolecular electron transfer in solution is comprised of the intramolecular component, λ_i, and the solvent component, λ_o, that is, $\lambda_T = \lambda_i + \lambda_o$.

The intramolecular contribution is calculated according to Marcus–Hush theory as the difference between the initial diabatic state with the electron located on donor (D or $A^{-\bullet}$) with the reactant in relaxed geometries and the final diabatic with the same molecular geometry but with the electron transferred to the acceptor ($D^{+\bullet}$or A), that is,

$$\lambda_i^{calcd} = \{E_c(r_n) + E_n(r_c)\} - \{E_n(r_n) + E_c(r_c)\} \qquad (13)$$

where r_n and r_c are the optimized coordinates and E_n and E_c are the energies of the donor and its counterpart.[20] Accordingly, we first optimize these geometries and determine their energies, $E_n(r_n)$ and $E_c(r_c)$ via DFT computations with aid of Gaussian 98 (6-311G* basis and B3LYP functional). Then the single-point calculation of acceptor in the geometry of the donor leads to $E_c(r_n)$, and the donor in the geometry of the acceptor produces $E_n(r_c)$. Typically, in $(TTF)_2^{+\bullet}$ the energy difference corresponds to $\lambda_i^{calcd} = 2.3 \times 10^3$ cm^{-1} or 6.8 kcal/mol.[19]

The solvent contribution to the reorganization energy has been successfully evaluated by the Marcus two-sphere model for non-adiabatic (or weakly adiabatic) electron transfer, especially of octahedral coordination redox dyads. However, we

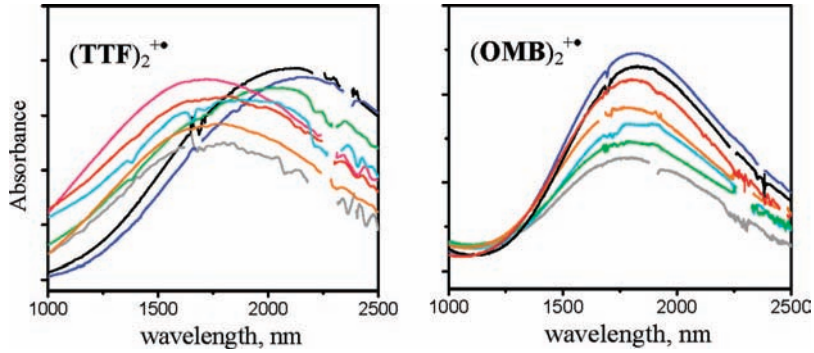

FIGURE 7. Electronic (NIR) spectra of $(TTF)_2^{+\bullet}$ (left) and $(OMB)_2^{+\bullet}$ (right) measured in $CHCl_3$ (blue), CH_2Cl_2 (black), acetone (red), CH_3CN (orange), tetrahydrofuran (THF, light blue), diethyl ether (green), propylene carbonate (PC, gray), and DMF (pink) (from ref 15).

find such computations to be generally inapplicable to Robin–Day class II and III encounter complexes consisting as they do of a pair of closely coupled redox centers of the type examined herein. Thus, in these dyads, the experimental solvent probe affects only class II encounter complexes, as typically illustrated for $(TTF)_2^{+\bullet}$ in Figure 7 (left); but under the same conditions the corresponding intervalence transition of class III, as represented by $(OMB)_2^{+\bullet}$ (OMB = octamethylbiphenylene) in Figure 7 (right), is essentially unaffected.[15]

With such a striking solvent differentiation of class II and III encounter complexes, we now treat solvation somewhat more realistically by computing λ_o as the free-energy change of the inertial solvent response to the solute cavity occupied by $D_2^{+\bullet}$ or $A_2^{-\bullet}$ by replacing the limiting Marcus outer-sphere model with

$$\lambda_o = G_s(\epsilon_{\infty 1}, \epsilon_{\infty 2}, \ldots, \epsilon_{\infty N}, \Delta q) - G_s(\epsilon_{01}, \epsilon_{02}, \ldots, \epsilon_{0N}, \Delta q) \quad (14)$$

where Δq is the point-charge representation of the full shift in the charge density in the encounter complex upon electron transfer.[21] As such, the dielectric continuum is based on the full solution of the Poisson equation for the solute cavity (described by the X-ray structure of either $D_2^{+\bullet}$ or $A_2^{-\bullet}$) immersed in the solvent environment of different dielectric zones with each characterized by an ϵ_0, ϵ_∞ pair. Indeed, the agreement of the intrinsic barriers calculated in this manner in Table 4 (columns 2 and 4) with those obtained from the experimental intervalence transition (columns 3 and 5) provides compelling validation of the X-ray structures (Table 2) to correctly predict the structural response of the critical encounter complex to the solvent environment.

TABLE 4. Quantitative Comparison of the Calculated Intrinsic Barrier with the Experimental Reorganization Energy Obtained from the Intervalence Absorption[a]

	TTF		TCNE	
solvent	λ_T(calcd)	λ_T(exptl)	λ_T(calcd)	λ_T(exptl)
chloroform	4.36	4.65		
tetrahydrofuran	5.29	5.13	5.81	6.67
dichloromethane	5.45	4.73	6.01	6.60
acetone	6.46	5.71	7.18	7.35
dimethylformamide	6.42	5.92	7.11	7.41
acetonitrile	6.82	5.81	7.62	7.25
propylene carbonate	6.62	5.71	7.34	7.37

[a] From ref 15.

7. Steric Inhibition Leading to Outer-Sphere Encounter Complexes

The resonance stabilization (H_{DA}) of the encounter complex plays a key role in lowering the activation barrier for electron transfer. Importantly, this attenuation is directly related to the red shift of the intervalence (or charge-transfer) absorption according to the Hush eq 12 that visually signals the existence of such an encounter complex. According to the expectations of Mulliken–Hush theory, the energy and intensity of the intervalence (charge-transfer) transition depicted in Chart 2 will be strongly attenuated by conceptually enlarging the interplanar separation (r_{DA}) between the planar cofacial dyads in the encounter complex.[22] This is experimentally

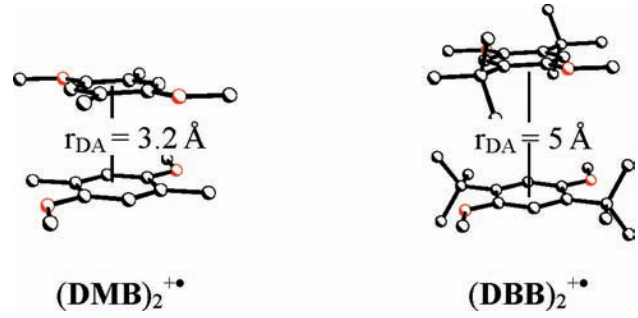

FIGURE 8. Comparison of r_{DA} for sterically open (left) and hindered (right) encounter complexes.

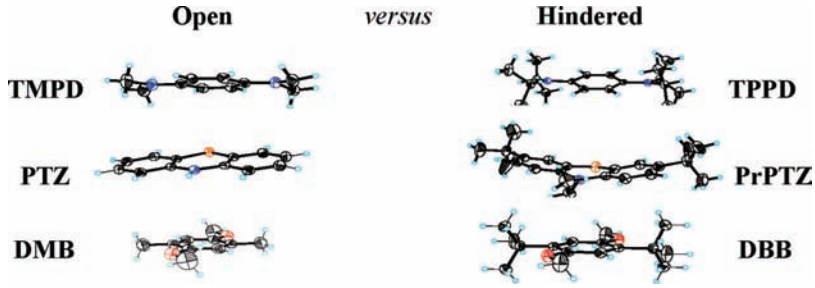

FIGURE 9. ORTEP structures of sterically open donors (left) and their hindered analogues (right).

achieved in the illustrative conversion of the 2,5-dimethylhydroquinone ether (DMB) to the analogous 2,5-di-*tert*-butyl donor (DBB) that results in the corresponding increase of r_{DA} from 3.2 to 5 Å in Figure 8.[9]

Indeed, such a steric effect is noted in the total absence of the intervalence band expected of the *t*-butyl-hindered $(DBB)_2^{+\bullet}$ under the same conditions that the methyl analogue DMB shows its strong CT absorption at $\lambda_{IV} = 1850$ nm ($\epsilon = 530\ M^{-1}\ cm^{-1}$). Similar steric inhibition of the encounter complex is encountered in the substituted phenylenediamine cation radical $TPPD^{+\bullet}$, as well as in the phenothiazine analogue $PrPTZ^{+\bullet}$ illustrated by the ORTEP diagrams in Figure 9, and we conclude that in each case, the encounter complex is too weak[23] for the experimental observation of the intervalence transition and will result in $H_{DA} < 200\ cm^{-1}$, which is characteristic of outer-sphere complexes.[9]

8. Modulation of the Electron-Transfer Kinetics by the Encounter Complex

The rather wide range of second-order electron-transfer rate constants that are available from the EPR broadening experiments accords well with the electron-transfer parameters (λ_T and H_{DA}) evaluated from the spectral measurements (as well as by computation) to allow the direct comparison sufficient to emphasize the critical importance of the precursor complex according to the generalized scheme in eq 3. Thus for the self-exchange processes in eq 9, the second-order rate constants for the bimolecular electron-transfer are described by

$$1/k_{SE} = 2/k_{diff} + 1/(K_{CT}k_{ET}) \qquad (15)$$

where k_{diff} is the diffusion rate constant, K_{CT} is the formation constant of the precursor complex, and $k_{ET} = \nu_n \exp(-\Delta G^*/(RT))$ is the first-order intracomplex electron-transfer rate constant. The activation barrier for the self-exchange electron transfer with $\Delta G^0_{ET} = 0$ is[5a,b]

$$\Delta G^* = (\lambda_T - 2H_{DA})^2/(4\lambda_T) \qquad (16)$$

The application of eqs 15 and 16, together with the reorganization energies and electron coupling energies for the various $D_2^{+\bullet}$ and $A_2^{-\bullet}$, leads to the calculated second-order rate constants presented in Table 5 (column 3), which are indeed in reasonable agreement with the experimental values (column 4) to underscore the kinetic (and mechanistic) importance of the encounter complex.[9,14] [Note that for the sterically hindered systems, the rate constants are approximated as $k_{SE} = Z \exp(-\Delta G^*/(RT))$, where $Z = 10^{11}\ M^{-1}\ s^{-1}$ is taken as the collision frequency.]

TABLE 5. Comparison of the Experimental and Calculated Rates Constants for Electron-Transfer Self-Exchange of Organic Ion Radicals[a]

ion radical	ΔG^*, (kcal/mol)	k_{SE}(calcd), ($10^9\ M^{-1}\ s^{-1}$)	k_{SE}(exptl), ($10^9\ M^{-1}\ s^{-1}$)	encounter complex[b]
$OMB^{+\bullet}$	0	3.2[c]	2.4	III
$OMA^{+\bullet}$	0	6.3[c]	2.5	III
$TMPD^{+\bullet}$	2.9	0.8	2.3	II
$TPPD^{+\bullet}$	6.2	0.003	0.01	OS[d]
$PTZ^{+\bullet}$	1.3	7.0	4.7	II
$PrPTZ^{+\bullet}$	3.2	0.4	0.3	OS[d]
$DMB^{+\bullet}$	2.2	1.0.	1.5	II
$DBB^{+\bullet}$	3.3	0.3	0.1	OS[d]
$TTF^{+\bullet}$	0.4	7.5	2.7	II
$TCNE^{-\bullet}$	2.2	10	4.3	II
$DDQ^{-\bullet}$	1.2	7.5	2.5	II/III
$TCNQ^{-\bullet}$	0.6	7.5	3.3	II/III

[a] In CH_2Cl_2, from ref 9. [b] According to Robin−Day classification unless noted otherwise. [c] The calculated difference is due to different experimental values of K_{CT}.[15] [d] OS = outer-sphere complex.

9. Generalized Mechanisms for Electron Transfer via the Energetic Differentiation among Encounter Complexes

Owing to the critical importance of the precursor complex in establishing the activation barrier and kinetics of the bimolecular electron transfer in eqs 15 and 16, let us consider how the potential-energy surface (PES) evolves from the two impor-

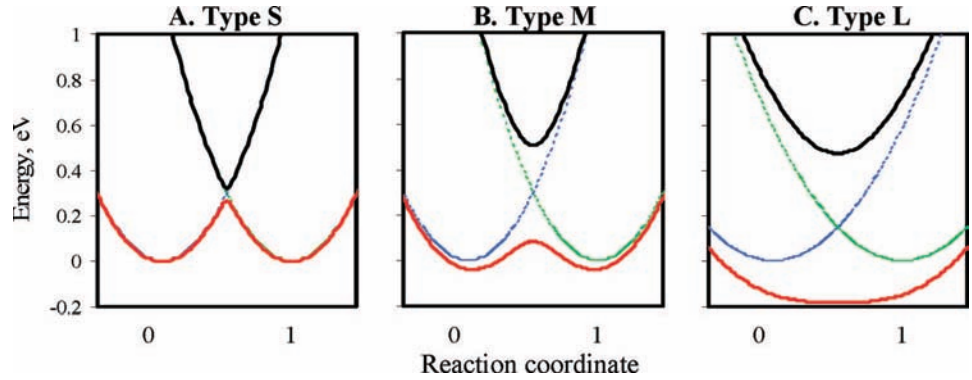

FIGURE 10. Potential-energy surfaces for self-exchange electron transfer (red) relative to the excited states (black) based on the two-state Mulliken−Hush formulation from ref 9.

tant electron-transfer parameters, H_{DA} and λ_T. According to Sutin,[5] the adiabatic ground-state and the excited-state energies are obtained from the two-state model via the intersection of the diabatic states at each point (X) along the reaction coordinate:

$$E_{GS,ES} = (H_{bb} + H_{aa})/2 \pm ((H_{bb} - H_{aa})^2 + 4H_{DA})^{1/2}/2 \quad (17)$$

where $H_{aa} = \lambda X^2$ and $H_{bb} = \Delta G_{ET} + \lambda(X - 1)^2$ represent the energies of the initial and final diabatic states.

The potential-energy diagrams in Figure 10 represent three limiting types of ground-state surfaces (in red) as defined by the magnitude of the electronic coupling energy within the particular encounter complex at the same value of the reorganization energy (λ_T).[9] The red curves are strongly differentiated at the intersection of the initial (blue) and final (green) diabatic curves to represent the change in the activation barrier, ΔG^0_{ET}, by the amount $\lambda_T - 2H_{DA}$ (eq 16), that is, the interplay between the "intrinsic" barrier, λ_T, and the "resonance" stabilization, H_{DA}. As such, the three limiting potential-energy surfaces in Figure 10 can be typically classified as (A) with $H_{DA} \ll \lambda/2$, (B) with $H_{DA} \leq \lambda/2$, and (C) with $H_{DA} > \lambda/2$.

Experimentally, Figure 10A is found for the sterically encumbered donor/acceptor dyads such as $(TPPD)_2^{+\bullet}$ with *small* H_{DA} values (<250 cm^{-1}), Figure 10B is found in $(TMPD)_2^{+\bullet}$ showing class II behavior with *medial* H_{DA} values (~1700 cm^{-1}), and Figure 10C shows the tightly bound $(OMB)_2^{+\bullet}$ displaying class III behavior with *large* H_{DA} values (~2500 cm^{-1}) when taken relative to λ_T (arbitrarily) set at 4000 cm^{-1}. As such, the Mulliken−Hush delineation of the potential-energy surfaces necessitates the reevaluation of the general mechanistic proposal in eq 3 into three distinctive mechanisms based on the magnitude of the resonance stabilization relative to the intrinsic barrier by quantitatively designating the donor/acceptor binding factor, $Q = 2H_{DA}/\lambda_T$, as the unique structural characteristic of each encounter complex.[9] [Note that the donor/acceptor binding factor is designated as Q owing to its direct relationship to the degree of charge transfer, q, which locates the encounter complex along the reaction coordinate, that is, $Q = (1 - (1 - 2q)^2)^{1/2}$ for $\Delta G^0_{ET} = 0$ and $Q < 1$.[11b]].

A. Weakly Coupled PES. Figure 10A encompasses sterically hindered encounter complexes in which the interplanar separation of $r_{DA} \approx 5-6$ Å is characterized by electronic coupling elements of $H_{DA} \approx 100-300$ cm^{-1}, and $Q \ll 1$. Their adiabatic (state) energies are likely to approximate those of the diabatic states, with notable deviations being only observed at or around the transition state. No significant resonance stabilization of the (strongly localized) ground state of the precursor complex is evident, and thus its formation constant is usually insufficient for experimental measurements. Indeed, all of these electron-transfer characteristics mirror those of the traditional (inorganic) outer-sphere mechanism,[2] and we conclude that at the limit of very weak H_{DA} couplings, the potential-energy surface in Figure 10A is therewith interchangeable.

B. Medially Coupled PES. Figure 10B applies to donor/acceptor dyads that are sterically and electronically open to rather intimate encounters with values of $r_{DA} = 3.0-3.3$ Å and $H_{DA} = 1000-3000$ cm^{-1} that result in substantial diminutions of the transition-state energies separating the localized (class II) encounter complex from the successor complex. Thus even for $(TMPD)_2^{+\bullet}$ with a relative low $2H_{DA}/\lambda_T$ ratio or with $0 < Q < 1$, the electron-transfer barrier is roughly halved relative to those in Figure 10A, and the significant ground-state stabilization leads to $K_{CT} \approx 0.1-1.0$ M^{-1}, which renders the encounter complex quite observable in solution. However, the self-exchange rate constants are close to the diffusion-controlled limit, and the evaluation of k_{SE} according to eq 15 leads to second-order rate constants in accord with those calculated in Table 5. The PES in Figure 10B includes the traditional (inorganic) inner-sphere or bridged mech-

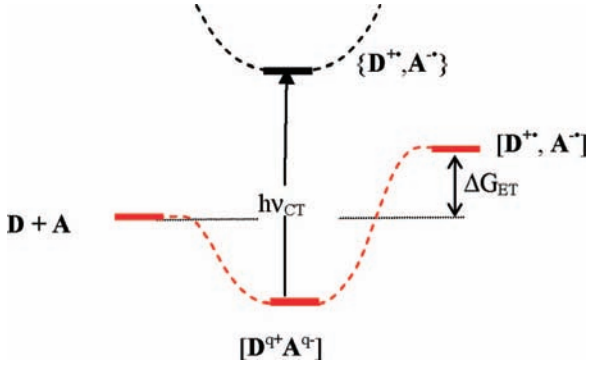

FIGURE 11. Schematic representation of the unique (barrierless) electron transfer proceeding via the strongly coupled encounter complex $[D^{q+}A^{q-}]$ with a high degree of charge transfer,[25] and its relationship to the non-adiabatic (charge-transfer) redox ion pair $\{D^{+\bullet}, A^{-\bullet}\}$ in eq 1 (from ref 12).

anism[2] and is predicted to cover a wide-ranging continuum of second-order rates.

C. Strongly Coupled PES. Figure 10C encompasses donor/acceptor dyads lying at the other extreme with large values of H_{DA} (relative to λ_T) or $Q \geq 1$, and the delocalized ground state consists of a single minimum.[24] As illustrated in Figure 10C, electron-transfer occurs in the absence of an activation barrier, being controlled by diffusive association/dissociation dynamics. Among electron-transfer mechanisms, the PES in Figure 10C is heretofore quite unprecedented because the odd-electron delocalization is predicted to actually coincide with the bimolecular encounter of freely diffusing D/A dyads.[12,25] Such a unique electron-transfer process is thus *barrierless* and driven directly to the adiabatic ion pair $[D^{+\bullet}/A^{-\bullet}]$ by the overall free-energy changes with $\Delta G^0_{ET} = F(E^0_{ox} - E^0_{red})$, as qualitatively depicted in Figure 11.[12]

According to this mechanistic formulation, the highly polarized encounter complex is the predominant (thermodynamic) species lying in a deep chemical "black hole"[12] and thus emergent to the non-adiabatic ion pair $\{D^{+\bullet}, A^{-\bullet}\}$ only upon direct photoexcitation ($h\nu_{CT}$) of the charge-transfer complex.[25] If such a mechanistic picture is valid for donor/acceptor dyads designated in eq 8 at or near the isergonic limit, the question then arises as to whether the charge-transfer state can coexist in reversible equilibrium with the electron-transfer state in the more general situation in which the ET driving force is substantially different from nil (see left drawing in Chart 2). In addition, we hope to direct our search to newer donor/acceptor systems that will identify other charge-transfer/electron-transfer interchanges that quantitatively describe the predicted localized inner-sphere with the double-minimum ground state predicted by Figure 10B.

10. Conclusions

The characteristic and ubiquitous intervalence absorption bands that accompany the diffusive encounter of electron donors (D) and acceptors (A) shed fresh insight into the behavior of various intermolecular encounter complexes by providing access to their important electron-transfer parameters: H_{DA} and λ_T. For purposes of mechanistic assignment, we designate the donor/acceptor binding factor, $Q = 2H_{DA}/\lambda_T$, as the basic structure parameter that defines various encounter complexes, so that $Q \ll 1$ identifies the weakly coupled systems that serve as the basis for the traditional outer-sphere electron transfer adequately served by non-adiabatic or weakly adiabatic Marcus theory. At the other extreme of large H_{DA} values with $Q \geq 1$, bimolecular electron transfer is uniquely spontaneous and heretofore unprecedented since Figure 11 shows that there is no activation barrier other than that pertaining to the diffusion-controlled encounter of donor/acceptor dyads. The inextensible intermediate region with $0 < Q < 1$ encompasses the classical Taube (ligand-based) bridged mechanism,[2] together with that of a wide variety of other donor/acceptor encounter complexes and offers for the first time an opportunity to quantitatively predict the rates of various other types of inner-sphere electron-transfer processes.

The three (left-to-right) drawings included in Figure 12 present a visual depiction of (a) the limiting outer-sphere mechanism, (b) the intermediary inner-sphere mechanism, and (c) the other limiting and unique diffusive "interior mechanism" that we hope will stimulate additional quantitative studies of the potentially wide variety of other organic and organometallic, as well as different inorganic and biochemical systems to further *chemical research into electron-transfer dynamics*.

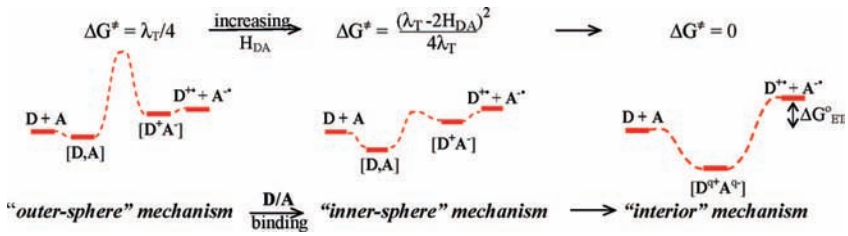

FIGURE 12. Three distinctive mechanisms for bimolecular electron transfer as progressively modulated by the donor/acceptor binding (H_{DA}) within the encounter complex (at constant λ_T).

11. Epilogue

For the structural definitions of outer-sphere and inner-sphere structures and mechanisms for organic in relation to inorganic redox dyads and their relevance to the energy relationship based on $Q = 2H_{DA}/\lambda_T$, see our extensive discussion in ref 9 (especially footnotes 6, 13, 14, 18, 53, 72, and 73 therein). Thus, in order to conciliate the inner-sphere mechanism based on donor/acceptor bindings (as presented herein) with those based on bridged activated complexes (of Taube[2]), it is important to recognize that this fundamental distinction boils down to the perception of "through-space" D, A interactions[14,26] versus "through-bond" D-bridge-A couplings[27] both of which have been shown to be equally amenable to theoretical treatment via the Mulliken−Hush two-state model.[28] Moreover, both types of encounter complexes exhibit the class II (localized) behavior for the "inner-sphere" mechanism, as well as the class III (delocalized) behavior for the "interior" mechanism.

We thank Marshall Newton and Noel Hush for their keen interest and generous help. We are grateful to Duoli Sun, Sergey Lindeman, Vellaichami Ganesan, Jian-Ming Lü, Almaz Jalilov, and JianJiang Lu for their invaluable assistance with the syntheses, X-ray structures, and spectral measurements, and the Robert A. Welch Foundation and National Science Foundation for their financial support. This Account is dedicated with deep appreciation to the Founding Editor Joe Bunnett on the felicitous occasion of his 86th birthday.

BIOGRAPHICAL INFORMATION

Sergiy V. Rosokha was born in Uzhgorod, Ukraine. He received his M.Sc. from the Moscow Institute for Physics and Technology and his Ph.D. from the Institute of Physical Chemistry of the Ukrainian Academy of Sciences. In 2000, he joined group of Prof. J. K. Kochi at University of Houston, where he is presently a Research Associate Professor.

Jay Kazuo Kochi is the Robert A. Welch Professor of Chemistry and a National Academy of Sciences member (1982).

FOOTNOTES

*To whom correspondence should be addressed. E-mail: jkochi@uh.edu.

REFERENCES

1 (a) Mulliken, R. S. Molecular compounds and their spectra. *J. Am. Chem. Soc.* **1952**, *74*, 811–824. (b) Mulliken, R. S.; Person, W. B. *Molecular Complexes. A Lecture and Reprint Volume*; Wiley: New York, 1969.

2 (a) Taube, H.; Myers, H. J.; Rich, R. L. The mechanism of electron transfer in solution. *J. Am. Chem. Soc.* **1953**, *75*, 4118–4119. (b) Taube, H. Electron transfer between metal complexes: Retrospective. *Science* **1984**, *226* (4678), 1028–1036.

3 (a) Marcus, R. A. The theory of oxidation-reduction reactions involving electron transfer. *J. Chem. Phys.* **1956**, *24*, 966–978. (b) Marcus, R. A. Electron-transfer reactions in chemistry: Theory and experiment (Nobel lecture). *Angew. Chem., Int. Ed.* **1993**, *32*, 1111–1121.

4 (a) Hush, N. S. Adiabatic theory of outer-sphere electron-transfer reactions in solutions. *Trans. Faraday Soc.* **1961**, *57*, 557–580. (b) Hush, N. S. Intervalence-transfer absorption. II. Theoretical considerations and spectroscopic data. *Prog. Inorg. Chem.* **1967**, *8*, 391–444.

5 (a) Sutin, N. Theory of electron transfer reactions: Insights and hindsights. *Prog. Inorg. Chem.* **1983**, *30*, 441–498. (b) Brunschwig, B. S.; Sutin, N. Energy surfaces, reorganization energies and coupling elements in electron transfer. *Coord. Chem. Rev.* **1999**, *187*, 233–254. (c) Compare also Piepho, S. B. Vibronic coupling model for the calculation of mixed-valence line shapes: A new look at the Creutz−Taube ion. *J. Am. Chem. Soc.* **1990**, *112*, 4197–4206.

6 (a) Kochi, J. K. Electron transfer and charge transfer: Toward the unification of organic and organometallic reaction mechanisms. *Angew. Chem., Int. Ed. Engl.* **1988**, *27*, 1227–1266. (b) Kochi, J. K. Inner-sphere electron transfer in organic chemistry. Relevance to electrophilic aromatic nitration. *Acc. Chem. Res.* **1992**, *25*, 39–47. (c) Gwaltney, S. R.; Rosokha, S. V.; Head-Gordon, M.; Kochi, J. K. Charge-transfer mechanism for electrophilic aromatic nitration and nitrosation via the convergence of (ab initio) molecular-orbital and Marcus-Hush theories with experiments. *J. Am. Chem. Soc.* **2003**, *125*, 3273–3283. (d) Kochi, J. K. Electron transfer in the thermal and photochemical activation of electron donor-acceptor complexes in organic and organometallic reactions. *Adv. Phys. Org. Chem.* **1994**, *29*, 185–272.

7 (a) Foster, R. *Organic Charge-Transfer Complexes*; Academic: New York, 1969. (b) See also Tamres, M., Strong, R. L. Contact charge-transfer spectra. In *Molecular Association*; Foster, R., Ed.; Academic Press: New York, 1979; Vol *2*, Chapter 5, pp 332–456. (c) Herbstein F. H. *Crystalline Molecular Complexes and Compounds: Structures and Principles*. Oxford University Press: New York, 2005.

8 (a) Hilinski, E. F.; Masnovi, J. M.; Amatore, C.; Kochi, J. K.; Rentzepis, P. M. Charge-transfer excitation of electron donor-acceptor complexes. Direct observation of ion pairs by time-resolved (picosecond) spectroscopy. *J. Am. Chem. Soc.* **1983**, *105*, 6167–6168. (b) Hilinski, E. F.; Masnovi, J. M.; Kochi, J. K.; Rentzepis, P. M. Role of ion pairs in the photochemistry of electron donor-acceptor complexes. Picosecond spectroscopic studies of arene-tetracyanoethylene systems. *J. Am. Chem. Soc.* **1984**, *106*, 8071–8077. (c) Masnovi, J. M.; Huffman, J. C.; Kochi, J. K.; Hilinski, E. F.; Rentzepis, P. M. Picosecond spectroscopy of charge-transfer processes. Photochemistry of anthracene-tetranitromethane EDA complexes. *Chem. Phys. Lett.* **1984**, *106*, 20–25.

9 Rosokha, S. V.; Kochi, J. K. Continuum of outer- and inner-sphere mechanisms for organic electron transfer. Steric modulation of the precursor complex in paramagnetic (ion-radical) self exchanges. *J. Am. Chem. Soc.* **2007**, *129*, 3683–3697.

10 Recently reviewed in Vasilyev, A. V.; Lindeman, S. V.; Kochi, J. K. Molecular structures of the metastable charge-transfer complexes of benzene (and toluene) with bromine as the pre-reactive intermediates in electrophilic aromatic bromination. *New J. Chem.* **2002**, *26*, 582–592.

11 (a) Rosokha, S. V.; Kochi, J. K. Mechanism of inner-sphere electron transfer via charge-transfer (precursor) complexes. Redox energetics of aromatic donors with the nitrosonium acceptor. *J. Am. Chem. Soc.,* **2001**, *123*, 8985–8999. (b) Rosokha, S. V.; Kochi, J. K. Strong electronic coupling in intermolecular (charge-transfer) complexes. Mechanistic relevance to thermal and optical electron transfer from aromatic donors. *New J. Chem.* **2002**, *26*, 851–860.

12 Rosokha, S. V. Sun, D. Kochi, J. K. Reversible interchange of charge-transfer *versus* electron-transfer states in organic electron transfer via cross-exchanges between diamagnetic (donor/acceptor) dyads. *J. Phys. Chem. B* **2007**, *111*, 6555–6666. See also ref 25.

13 Ward, R. L.; Weissman, S. I. Electron-spin resonance study of the electron exchange between naphthalene negative ion and naphthalene. *J. Am. Chem. Soc.* **1957**, *79*, 2086–2090.

14 Ganesan, V.; Rosokha, S. V.; Kochi, J. K. Isolation of the latent precursor complex in electron-transfer dynamics. Intermolecular association and self-exchange with acceptor anion radicals. *J. Am. Chem. Soc.* **2003**, *125*, 2559–2571.

15 Rosokha, S. V.; Newton, M. D.; Jalilov, A. S.; Kochi, J. K. The spectral elucidation versus the X-ray structure of the critical precursor complex in bimolecular electron transfers: Application of experimental/theoretical solvent probes to ion-radical (redox) dyads. *J. Am. Chem. Soc.* **2008**, *130*, 1944–1952.

16 Robin, M. B.; Day, P. Mixed valence chemistry. A survey and classification. *Adv. Inorg. Chem. Radiochem.* **1967**, *10*, 247–422. See also Sun, D.; Rosokha, S. V.; Kochi, J. K. Donor-acceptor (electronic) coupling in the precursor complex to organic electron transfer: intermolecular and intramolecular self-exchange between phenothiazine redox centers. *J. Am. Chem. Soc.* **2004**, *126*, 1388–1401.

17 Creutz, C.; Newton, M. D.; Sutin, N. Metal-ligand and metal-metal coupling elements. *J. Photochem. Photobiol. A: Chem.* **1994**, *82*, 47–59.

18 Newton, M. D. Quantum chemical probes of electron-transfer kinetics: the nature of donor-acceptor interactions. *Chem. Rev.* **1991**, *91*, 767–792.

19 Rosokha, S. V.; Kochi, J. K. Molecular and electronic structures of the long-bonded π-dimers of tetrathiafulvalene cation radical in intermolecular electron transfer and in (solid-state) conductivity. *J. Am. Chem. Soc.* **2007**, *129*, 828–838.

20 See, for example: (a) Rosokha, S. V.; Lü, J.-M.; Newton, M. D.; Kochi, J. K. Intermolecular electron-transfer mechanisms via quantitative structures and ion-pair equilibria for self-exchange of anionic (dinitrobenzenide) donors. *J. Am. Chem. Soc.* **2005**, *127*, 7411–7420. (b) Rosokha, S. V.; Newton, M. D.; Head-Gordon, M.; Kochi, J. K. Mulliken-Hush elucidation of the encounter (precursor) complex in intermolecular electron transfer via self-exchange of tetracyanoethylene anion-radical. *Chem. Phys.* **2006**, *324*, 117–128.

21 Liu, Y.-P.; Newton, M. D. Solvent reorganization and donor/acceptor coupling in electron-transfer processes: self-consistent reaction field theory and ab initio applications. *J. Phys. Chem.* **1995**, *99*, 12382–12386.

22 See: (a) Fukuzumi, S.; Wong, C. L.; Kochi, J. K. Unified view of Marcus electron transfer and Mulliken charge transfer theories in organometallic chemistry. Steric effects in alkylmetals as quantitative probes for outer-sphere and inner-sphere mechanisms. *J. Am. Chem. Soc.* **1980**, *102*, 2928–2939. (b) Fukuzumi, S.; Kochi, J. K. Importance of work terms in the free energy relationship for electron transfer. *Bull. Chem. Soc. Jpn.* **1983**, *56*, 969–979.

23 (a) Rathore, R.; Lindeman, S. V.; Kochi, J. K. Charge-transfer probes for molecular recognition via steric hindrance in donor-acceptor pairs. *J. Am. Chem. Soc.* **1997**, *119*, 9393–9404. (b) Hubig, S. M.; Rathore, R.; Kochi, J. K. Steric control of electron transfer. Changeover from outer-sphere to inner-sphere mechanisms in arene/quinone redox pairs. *J. Am. Chem. Soc.* **1999**, *121*, 617–626.

24 Lindeman, S. V.; Rosokha, S. V.; Sun, D.-L.; Kochi, J. K. X-ray structure analysis and intervalent electron transfer in organic mixed-valence crystals with bridged aromatic cation radicals. *J. Am. Chem. Soc.* **2002**, *124*, 843–855.

25 Rosokha, S. V.; Dibrov, S. M.; Rosokha, T. Y.; Kochi, J. K. Electronic structures of intermolecular charge-transfer states in fast electron transfers with tetrathiafulvalene donor. Thermal and photoactivation of [2 + 4] cycloaddition to *o*-chloranil acceptor. *Photochem. Photobiol. Sci.* **2006**, *5*, 914–924.

26 Clayton, A. H. A.; Scholes, G. D.; Ghiggino, K. P.; Paddon-Row, M. N. Through-bond and through-space coupling in photoinduced electron and energy transfer: An ab initio and semiempirical study. *J. Phys. Chem.* **1996**, *100*, 10912–10918.

27 Creutz, C. Mixed valence complexes of d5-d6 metal centers. *Prog. Inorg. Chem.* **1983**, *30*, 1–73.

28 Sun, D.-L.; Rosokha, S. V.; Lindeman, S. V.; Kochi, J. K. Intervalence (charge-resonance) transitions in organic mixed-valence systems. Through-space versus through-bond electron transfer between bridged aromatic (redox) centers. *J. Am. Chem. Soc.* **2003**, *125*, 15950–15963.